A Comparative Study of Several Wind Estimation Algorithms for Spaceborne Scatterometers

CHONG-YUNG CHI, MEMBER, IEEE, AND FUK K. LI

Abstract—Using the radar backscattering coefficient (σ_o) measurements over the ocean surface by a spaceborne scatterometer, one can estimate the near-surface wind by using a geophysical model that relates σ_o to winds and a wind estimation algorithm. The so-called SOS algorithm, which is basically an algorithm with weighted least squares in the log domain (WLSL), was used to process the Seasat SASS data. In this paper, we compare the performances of seven wind estimation algorithms, including the WLSL, maximum-likelihood (ML), least squares (LS), weighted least squares (WLS), adjustable weighted least squares (AWLS), L1 norm, and least wind speed squares (LWSS) algorithms, for wind retrieval. For each algorithm, we present performance simulation results for the NASA scatterometer (NSCAT) [4] system planned to be launched in the 1990's. A relative performance merit based on the root mean square value of wind vector error is devised for this comparison study. According to this merit, performances for all algorithms are quite comparable. However, the results do indicate that the ML algorithm performs best for the 50-km wind resolution cell case and the L1 norm algorithm performs best for the 25-km wind resolution cell case. We have also considered preaveraging the σ_o measurements obtained from each antenna beam for the 50-km resolution wind cell case. The performances of all algorithms are even more similar in these cases with preaveraging, although the L1 norm algorithm performs best. Finally, the issue of using a two-stage wind estimation method in order to reduce the computational load and its impact on algorithm performance are discussed.

I. Introduction

THE DATA FROM many aircraft scatterometer experiments and the SEASAT Scatterometer (SASS) [1], [2] demonstrated that the radar backscattering coefficient σ_o over the ocean can be used to infer near-surface oceanic winds through a geophysical model function (examples of the model function are given in [1]–[3]). An interesting characteristic of the geophysical model function is the double sinusoidal relationship between σ_o and the relative azimuth angle (the angle between the wind direction and the azimuth angle of the radar observation). Thus, at least two σ_o measurements from two different azimuths are required to determine the wind speed and wind direction.

The existing geophysical model functions are nonlinear functions of wind speed, wind direction, antenna polarization, relative azimuth angle, and incidence angle. The inversion of σ_o measurements to wind vector is not necessarily straightforward because of the existence of various noise sources in the σ_o measurements in addition to the nonlinearity of the model function. The so-called sum-of-square (SOS) algorithm first developed by Wentz [2], which is basically a weighted least squares algorithm with σ_o expressed in the log domain (WLSL), was used to estimate the wind vector for SASS data. However, the algorithm has significant drawbacks in cases with low signal-to-noise ratios. In such cases, the estimated σ_o could be negative due to fluctuations in the system signal and noise power measurements. Since SASS obtained only two σ_o measurements for each 50-km resolution wind cell that were 90 degrees apart in azimuth, if one or both σ_o's were negative, the wind estimation could not be performed. This could lead to significant biases in the global wind results. A maximum-likelihood (ML) algorithm in wind estimation was then considered by Pierson [8]. He reported that the ML algorithm worked well without any limitations in the values of σ_o measurements.

As a follow-on to the SASS system, the NASA scatterometer (NSCAT) is being developed for launch in the early 1990's [4]. A key improvement in NSCAT is the use of three antennas on each side of the subsatellite track to provide σ_o measurements from three, instead of two, azimuthal angles. Furthermore, the center antenna will be dual-polarized, so that four σ_o sets will be obtained from the three antennas. The σ_o measurements will have a spatial resolution of 25 km. It is envisioned that the σ_o measurements will be combined to obtain wind vector estimates with resolutions of 25 and 50 km. Four σ_o measurements will be used for the 25-km case whereas 16 σ_o measurements will be used for the 50-km case. Due to these system improvements and the inadequacy mentioned above for the SOS algorithm, we have conducted a systematic study of seven potential wind retrieval algorithms for NSCAT data processing. The seven algorithms are WLSL, ML, least squares (LS), weighted least squares (WLS), adjustable weighted least squares (AWLS), L1 norm, and least wind speed squares (LWSS) algorithms. Among these seven algorithms, only the LWSS algorithm cannot be found in classical estimation literature (see Section III).

In Section II, we describe the assumptions including the model function, the noise variance in the σ_o measurement, etc., that were made in our study. We describe the seven wind estimation algorithms including the objective functions, computational loads, and other limitations in Section III. In Section IV, we present the simulation results

Manuscript received June 9, 1987; revised November 16, 1987. This work was supported by the National Aeronautics and Space Administration.

The authors are with the Jet Propulsion Laboratory, California Institute of Technology, Pasadena, CA 91109.

IEEE Log Number 8719109.

on the performance of these seven algorithms in terms of wind vector error for three different swath locations in the NSCAT design. We rank each algorithm based on the performance merits obtained. We also studied the use of "preaveraging" σ_o measurements obtained from each antenna beam, before the wind estimation. Finally, we draw conclusions based on these simulation results and discuss the use of a two-stage wind estimation method in order to reduce the computational load and its impact on algorithm performance.

II. Simulation Assumption

An estimation algorithm is generally optimal in the sense of minimizing a cost function or an objective function, which is a convex function of the residual between the measurements and the system model. The error variance of measurements is important to almost every estimation algorithm. They are usually used to weight the residuals in the objective function. Therefore, before we describe the wind estimation algorithms, we present the model for the noise variance in σ_o measurement.

The σ_o measurement $\hat{\sigma}_o$ is assumed to be the sum of the true σ_o and a random noise n

$$\hat{\sigma}_o = \sigma_o + n. \tag{1}$$

σ_o is related to the wind through the geophysical model function. The first geophysical model function used in this study was the SASS-I model, which is given by

$$\sigma_o = 10^G U^H \tag{2}$$

where U is the wind speed, and G and H are two coefficients that depend on the wind direction ϕ, the antenna azimuth angle, the incidence angle, and the antenna polarization (vertical or horizontal) (see [2]). Note that the wind direction ϕ is implicit in the G and H coefficients and that the model function is nonlinear in wind speed. Equation (2) can be expressed in log domain by

$$\log \sigma_o = G + H \log U. \tag{3}$$

One can see that for the SASS-I model, $\log \sigma_o$ is a linear function of $\log U$ (the standard form of the SASS model function is expressed in the decibel domain, which is 10 times that given in (3)).

The normalized standard deviation of $\hat{\sigma}_o$, denoted by $K_P(\sigma_o)$, is defined by

$$K_P(\sigma_o) = \left\{ \frac{\text{Var}[\hat{\sigma}_o]}{\sigma_o^2} \right\}^{1/2}. \tag{4}$$

Thus, $K_P(\sigma_o)$ indicates the accuracy of the σ_o measurement. The noise n in the normal domain is assumed to be a Gaussian random variable with zero mean. Chi, Long, and Li [5] presented a derivation of the K_P equation associated with the NSCAT digital Doppler processing system. The derived K_P equation is a quadratic function of the signal-to-noise ratio (SNR). Therefore, the variance can be expressed as (through the radar equation of $\hat{\sigma}_o$)

$$\text{Var}[\hat{\sigma}_o] = \alpha\sigma_o^2 + \beta\sigma_o + \gamma. \tag{5}$$

We note that $\text{Var}[\hat{\sigma}_o]$ and $K_P(\sigma_o)$ cannot be computed from σ_o measurements because they are functions of the true σ_o's.

III. Wind Estimation Algorithms

Assume that $N \sigma_o$ measurements, denoted $\hat{\sigma}_{oi}$ for $i = 1, 2, \cdots, N$ are available for wind estimation. From here on, any quantity with subscript i is associated with $\hat{\sigma}_{oi}$. Let us define the residuals of σ_{oi} and U either in the log domain or in the normal domain by the following:

$$a_i = \hat{\sigma}_{oi} - \sigma_{oi}. \tag{6}$$

$$b_i = \log \hat{\sigma}_{oi} - \log \sigma_{oi} \tag{7}$$

$$c_i = \log \hat{U}_i - \log U \tag{8}$$

and

$$d_i = \hat{U}_i - U \tag{9}$$

where

$$\hat{U}_i = 10^{((\log \hat{\sigma}_{oi} - G_i)/H_i)} \tag{10}$$

with $\hat{\sigma}_{oi} > 0$. Let $f_{oi}(\sigma_{oi})$, $f_{bi}(\sigma_{oi})$, $f_{ci}(\sigma_{oi})$, and $f_{di}(\sigma_{oi})$ denote the variances of a_i, b_i, c_i, and d_i, respectively. Notice, from (1), (4), and (6), that $f_{ai}(\sigma_{oi}) = \text{Var}[\hat{\sigma}_{oi}]$. From (2) through (4) and (7) through (9), one can see that for small K_P

$$\begin{aligned} f_{bi}(\sigma_{oi}) &= \text{Var}[b_i] \cong \text{Var}[\partial(\log \sigma_{oi})] \\ &= \left(\frac{1}{\ln 10}\right)^2 \text{Var}\left[\frac{\partial \sigma_{oi}}{\sigma_{oi}}\right] \\ &\cong \left(\frac{1}{\ln 10}\right)^2 K_{Pi}^2(\sigma_{oi}) \end{aligned} \tag{11}$$

$$\begin{aligned} f_{ci}(\sigma_{oi}) &= \text{Var}[c_i] \cong \text{Var}[\partial(\log U)] \\ &= \text{Var}\left[\left(\frac{1}{\ln 10}\right) \frac{1}{H_i} \frac{\partial \sigma_{oi}}{\sigma_{oi}}\right] \\ &\cong \left(\frac{1}{\ln 10}\right)^2 \left(\frac{1}{H_i}\right)^2 K_{Pi}^2(\sigma_{oi}) \end{aligned} \tag{12}$$

and

$$\begin{aligned} f_{di}(\sigma_{oi}) &= \text{Var}[d_i] \cong \text{Var}[\partial U] \\ &= \text{Var}\left[\left(\frac{U}{H_i}\right) \frac{\partial \sigma_{oi}}{\sigma_{oi}}\right] \cong \left(\frac{U}{H_i}\right)^2 K_{Pi}^2(\sigma_{oi}). \end{aligned} \tag{13}$$

We note that $f_{ai}(\sigma_{oi})$, $f_{bi}(\sigma_{oi})$, $f_{ci}(\sigma_{oi})$, and $f_{di}(\sigma_{oi})$ are functions of true σ_{oi} rather than $\hat{\sigma}_{oi}$.

The objective function of our estimators is given by the functional form

$$J(U, \phi) = \sum_{i=1}^{N} \left| \frac{e_i}{\delta_i} \right|^p + q \ln \delta_i^p. \tag{14}$$

The parameters p, q, e_i, and δ_i for each of the seven algorithms are given by the following:

1) WLSL algorithm:
$p = 2, q = 0, e_i = b_i$, and $\delta_i^2 = f_{bi}(\hat{\sigma}_{oi})$ or $e_i = c_i$ and $\delta_i^2 = f_{ci}(\hat{\sigma}_{oi})$.
2) ML algorithm:
$p = 2, q = 1, e_i = a_i$, and $\delta_i^2 = f_{ai}(\sigma_{oi})$.
3) LS algorithm:
$p = 2, q = 0, e_i = a_i$, and $\delta_i^2 = 1$.
4) WLS algorithm:
$p = 2, q = 0, e_i = a_i$, and $\delta_i^2 = f_{ai}(\hat{\sigma}_{oi})$.
5) AWLS algorithm:
$p = 2, q = 0, e_i = a_i$, and $\delta_i^2 = f_{ai}(\sigma_{oi})$.
6) L1 algorithm:
$p = 1, q = 0, e_i = a_i$, and $\delta_i^2 = f_{ai}(\hat{\sigma}_{oi})$.
7) LWSS algorithm:
$p = 2, q = 0, e_i = d_i$, and $\delta_i^2 = f_{di}(\hat{\sigma}_{oi})$.

Let us clarify the notational confusion for $f_{ai}(\hat{\sigma}_{oi})$, $f_{bi}(\hat{\sigma}_{oi})$, $f_{ci}(\hat{\sigma}_{oi})$, $f_{di}(\hat{\sigma}_{oi})$, and $f_{ai}(\sigma_{oi})$ used in these seven algorithms by stating that $f_{ai}(\sigma_{oi}) = f_{ai}(x)$ for $x = \sigma_{oi}$ and $f_{ai}(\hat{\sigma}_{oi}) = f_{ai}(x)$ for $x = \hat{\sigma}_{oi}$. All the objective functions are based on the classic estimation techniques except the LWSS algorithm. The wind speed U and direction ϕ are implicit in the above objective functions through the geophysical model function. The residuals inside the summation of each individual objective function are weighted by a positive quantity. All the above algorithms try to fit the $\hat{\sigma}_o$ to the geophysical model function with the $\hat{\sigma}_o$ expressed either in the normal domain or in the log domain. The WLSL algorithm also attempts to fit the data to the true wind speed U in the log domain. This feature motivated us to study the LWSS algorithm, which performs the same estimation in the normal domain. The wind direction is implicit in $\hat{U}_i$ (see (10)), which is uniquely determined by $\hat{\sigma}_{oi}$ for a given wind direction. The objective function of the ML algorithm is just the negative log function of the probability density function of $p(\hat{\sigma}_{oi}, i = 1, 2, \cdots, N | U, \phi)$.

The parameter δ_i determines the relative weight for each σ_o measurement. It is logical that noisier measurements should be given less weight in the objective function (larger δ_i). We emphasize that the noise variance and the K_P value are functions of the true σ_o, which is an unknown quantity. A simple way to estimate these values is to substitute the $\hat{\sigma}_{oi}$ into the equation of Var $[e_i]$ (albeit it is not necessarily appropriate in a statistical estimation sense). The weights of the WLSL, WLS, L1, and LWSS algorithms are based on this rationale and can be computed once $\hat{\sigma}_{oi}$ is given. The ML and AWLS algorithms treat the residual variance as a function of the true σ_o instead of a fixed quantity computed from the $\hat{\sigma}_o$. The LS algorithm treats all σ_o measurements equally (i.e., no weighting).

The parameter δ_i for the LWSS algorithm is a function of the unknown quantity U. However, the objective function J_{LWSS} can also be expressed as

$$J_{LWSS}(U, \phi) = \sum_{i=1}^{N} \left(\frac{1}{U} - \frac{1}{\hat{U}_i}\right)^2 \frac{\hat{U}_i^2 H_i^2}{K_{Pi}^2(\hat{\sigma}_{oi})} \quad (15)$$

which is a quadratic function of $1/U$, and $\hat{U}_i^2 H_i^2 / K_{Pi}^2(\hat{\sigma}_{oi})$ can be computed from $\hat{\sigma}_{oi}$. Therefore, when the wind direction is given or fixed, the LWSS algorithm has a closed form solution for U

$$U_{LWSS} = \frac{T_2}{T_1} \quad (16)$$

where

$$T_1 = \sum_{i=1}^{N} \frac{\hat{U}_i H_i^2}{K_{Pi}^2(\hat{\sigma}_{oi})} \quad (17)$$

and

$$T_2 = \sum_{i=1}^{N} \frac{\hat{U}_i^2 H_i^2}{K_{Pi}^2(\hat{\sigma}_{oi})}. \quad (18)$$

In addition, the wind speed solution for the WLSL algorithm is also known to be

$$U_{WLSL} = 10^{S_2/S_1} \quad (19)$$

where

$$S_1 = \sum_{i=1}^{N} \frac{H_i^2}{K_{Pi}^2(\hat{\sigma}_{oi})} \quad (20)$$

and

$$S_2 = \sum_{i=1}^{N} \frac{(\log \hat{\sigma}_{oi} - G_i) H_i}{K_{Pi}^2(\hat{\sigma}_{oi})}. \quad (21)$$

Due to the existence of these closed form solutions, the computational load for these two algorithms is much smaller than for the other algorithms, which must solve for the wind speed by a nonlinear numerical method. However, these two algorithms use the log function of $\hat{\sigma}_{oi}$ for the wind estimation and, therefore, nonpositive $\hat{\sigma}_{oi}$'s are precluded from the wind estimation process.

The other algorithms do not have a closed form solution for wind speed even when the wind direction is given. Many numerical methods can be used to search for the optimal wind speed. The method used in this paper is a gradient-type iterative search method, called the "Marquardt-Levenberg" algorithm [11], [12]. The wind speed U_{i+1} at the $(i + 1)^{\text{th}}$ iteration is updated by

$$U_{i+1} = U_i - (H_i + D_i)^{-1} g_i \quad (22)$$

where g_i denotes the gradient

$$g_i = \left.\frac{\partial J}{\partial U}\right|_{U = U_i} \quad (23)$$

H_i denotes the Hessian

$$H_i = \left.\frac{\partial^2 J}{\partial U^2}\right|_{U = U_i} \quad (24)$$

J denotes the objective function, D_i is chosen such that $(H_i + D_i)$ is positive definite, and $J(U_{i+1}) < J(U_i)$. Of course, a first guess of U_0 is required to initialize this algorithm. Wind solutions can be obtained by searching for wind speeds using the Marquardt–Levenberg algorithm, and searching for wind directions using a fixed interval method.

IV. Computer Simulations of Algorithm Performance

In this section, we present some computer simulations for the seven wind estimation algorithms using parameters associated with the NSCAT system. In the NSCAT design, three fan-beam antennas with azimuth angles 45, 115, and 135 degrees relative to the subsatellite direction will be used on both sides of the subsatellite track. Each antenna beam provides 1 σ_o measurement with 25-km resolution at a cross track spacing of 25 km. For the processing of the NSCAT data by the NASA research processing system, wind vector cells of 50-km resolution will be generated. A grouping procedure will be used for collecting the σ_o measurements associated with a wind cell from the multiple antenna beams before retrieving wind.

We will present the simulation results for three swath locations (near, mid, and far) in which the incidence angles of the σ_o measurements with the 45/135 degree antenna beams are 20, 41, and 58 degrees, respectively. Three different wind speeds (3, 8, and 25 m/s) were studied. The wind directions were chosen randomly from a uniform distribution of 0 to 360 degrees. We also present the simulation results for the case in which both the wind speed and wind direction were generated randomly. In this case, the distribution of wind speeds was chosen to be Rayleigh distributed with a mean of 8 m/s.

The variance Var $[\hat{\sigma}_o]$ used in these simulations includes the communication noise, a model function error, and uncertainties due to spacecraft attitude, antenna pointing, etc.. The detailed computation of this total variance will be reported in a separate paper. The α, β, and γ coefficients in the quadratic noise variance equation (5) used in these simulations are shown in Table I. In this table, each set of α, β, and γ values is associated with a separate antenna and swath location. For the 25-km wind cell case, the first set of α, β, and γ was used to generate σ_o measurements. For the 50-km wind cell case, the first set of α, β, and γ from each antenna was used for $2\sigma_o$ measurements and the other set of α, β, and γ was used for the other $2\sigma_o$ measurements. The simulations proceeded as follows: for an input wind speed and wind direction the true σ_{oi} was computed based on the SASS-I model function; a gaussian random noise with the variance computed using (5) was then generated by a random number generator; the $\hat{\sigma}_{oi}$ was obtained by adding the noise to the true σ_{oi}; a wind vector was then retrieved by each of the seven algorithms. The wind vector error $\vec{e}$ is defined as follows:

$$\vec{e} = \vec{V} - \hat{\vec{V}} \tag{25}$$

where $\vec{V}$ is the true wind vector and $\hat{\vec{V}}$ is the estimated wind vector. Usually, two to four wind solutions, called ambiguities, were obtained using the wind estimation algorithm. The ambiguity that was closest to the true wind vector among all ambiguities was chosen to be the estimated wind vector in our simulations. The statistical rms error for $|\vec{e}|$, denoted e_{RMS}, was computed by averaging over 10 000 independent wind estimations. The simulation results for all the algorithms studied were obtained using the same set of $\hat{\sigma}_{oi}$ data. Although the current NSCAT wind measurement accuracy is specified in terms of wind speed measurement accuracy and wind direction measurement accuracy, we used the wind vector error instead of the wind speed error and the wind direction error in this comparison study. The reason is that it is difficult to compare any two algorithms when the wind speed error is smaller for one algorithm and the wind direction error is smaller for the other algorithm or vice versa. Since wind vector error is a combination of wind speed and direction error, this dilemma will not occur.

TABLE I
α, β, and γ Values in the Noise Variance Expression

Ant (no.)	NEAR α $\times 10^{-2}$	NEAR β $\times 10^{-3}$	NEAR γ $\times 10^{-3}$	MID α $\times 10^{-2}$	MID β $\times 10^{-5}$	MID γ $\times 10^{-6}$	FAR α $\times 10^{-2}$	FAR β $\times 10^{-5}$	FAR γ $\times 10^{-7}$
1	4.58	1.87	1.67	4.84	7.44	1.05	5.29	6.96	4.93
	4.61	1.50	1.01	4.88	6.87	0.79	5.40	8.78	6.70
2	4.80	3.08	1.48	5.04	12.5	1.76	5.18	5.12	1.88
	4.71	2.51	0.99	5.00	10.5	1.11	5.17	4.69	1.77
3	4.58	1.87	1.67	4.84	7.44	1.05	5.31	7.40	5.21
	4.60	1.50	1.01	4.88	6.87	0.79	5.39	8.78	6.71

Table II shows the simulation results for wind speeds of 3, 8, and 25 m/s. From this table, one observes that the performances for all the algorithms are quite comparable. No single algorithm was obviously far superior or inferior to the others. One can also see that the performance of each algorithm is better for the 50-km resolution case than for the 25-km resolution case. This is intuitive because 16-σ_o measurements were used for the 50-km resolution cell rather than 4-σ_o measurements for the 25-km resolution cell. The performance is best at the mid swath location while the performance at the far swath is better than at the near swath except for the case with 3 m/s wind speed. The second set of simulation results are for both random wind speeds and wind directions; the results are shown in Table III. One can observe, again, that the performance at the mid swath is the best and the performance at the far swath is the second best. The performance is determined by the SNR or K_P values and the wind sensitivity of the geophysical model (absolute H values in the SASS-I model). The performance is better for smaller K_P values and for larger wind sensitivity. Both the K_P values and the wind sensitivity increase from the near swath through the far swath. The combination of K_P values and $|H|$ values results in best performance at the mid swath location.

We have evaluated the standard deviation of the simulation results with a 10 000-sample size by using different sequences of random numbers and found that it is about 2.5 percent of the simulation results. For each simulation case (three swath locations and three wind speeds), we

TABLE II
PERFORMANCE SIMULATION RESULTS e_{RMS} (IN METERS PER SECOND) FOR FIXED WIND SPEED CASE

	25 KM			50 KM		
ALG.	NEAR	MID	FAR	NEAR	MID	FAR
	wind speed 3 m/s					
WLSL	1.32	1.34	2.03	0.87	0.92	1.68
ML	1.30	1.11	1.60	0.80	0.66	1.07
LS	1.45	1.05	1.64	0.93	0.67	1.10
WLS	1.43	1.14	1.61	1.01	0.74	1.12
AWLS	1.35	1.14	1.63	0.86	0.69	1.10
L1	1.27	0.98	1.39	0.87	0.63	1.02
LWSS	1.44	1.39	2.19	1.06	1.02	2.02
	wind speed 8 m/s					
WLSL	2.85	1.65	1.84	1.56	0.89	1.00
ML	2.78	1.65	1.81	1.52	0.85	0.96
LS	3.40	1.84	2.18	1.96	1.10	1.21
WLS	3.14	1.83	2.01	2.14	1.31	1.42
AWLS	2.89	1.65	1.80	1.65	0.89	0.99
L1	2.82	1.57	1.67	1.78	0.98	1.11
LWSS	2.97	1.62	1.87	1.79	0.87	1.04
	wind speed 25 m/s					
WLSL	8.11	6.56	7.81	4.45	3.71	4.52
ML	7.71	6.49	7.55	4.17	3.44	4.00
LS	8.59	7.18	8.99	4.67	4.11	4.82
WLS	8.77	7.41	8.90	6.19	5.52	6.71
AWLS	8.12	6.43	7.54	4.50	3.52	4.11
L1	7.83	6.25	7.17	5.02	4.09	4.87
LWSS	8.32	6.44	7.66	4.84	3.49	4.23

TABLE III
PERFORMANCE SIMULATION RESULTS e_{RMS} (IN METERS PER SECOND) FOR THE CASE THAT BOTH WIND SPEEDS AND WIND DIRECTIONS ARE RANDOM

	25 KM			50 KM		
ALG.	NEAR	MID	FAR	NEAR	MID	FAR
WLSL	3.13	2.07	2.38	1.74	1.20	1.49
ML	3.02	2.04	2.22	1.67	1.06	1.20
LS	3.60	2.22	2.62	2.07	1.35	1.52
WLS	3.40	2.20	2.48	2.37	1.62	1.81
AWLS	3.17	2.03	2.22	1.81	1.11	1.24
L1	3.06	1.93	2.10	1.97	1.25	1.40
LWSS	3.26	2.06	2.40	1.95	1.17	1.58

give each algorithm a merit M defined as follows:

$$M = \begin{cases} 1 & e_{RMS} \leq 1.05 \cdot \min(e_{RMS}) \\ 0 & \text{otherwise} \end{cases} \tag{26}$$

where $\min(e_{RMS})$ is the minimum value of e_{RMS} among all the seven algorithms. Finally, the seven algorithms were ranked using the accumulated M values over all the simulation cases. The ranks for both the 25-km resolution and the 50-km resolution cases are shown in Table IV. One can see that the ML algorithm was ranked the best for the 50-km resolution case and the L1 algorithm was ranked the best for the 25-km resolution case.

Next, we present the results when the σ_o measurements were "preaveraged" within a 50-km wind cell. For each antenna beam, the preaveraged σ_o measurement $\overline{\sigma_o}$ is defined as the arithmetic average of all the σ_o measurements within the 50-km resolution wind cell

$$\overline{\sigma_o} = \frac{1}{M} \sum_{i=1}^{M} \hat{\sigma}_{oi} \tag{27}$$

where M is the number of σ_o measurements, and σ_{oi}'s are the 25-km σ_o measurements. Similarly, the incidence angle and azimuth angles associated with $\overline{\sigma_o}$ are defined as the arithmetic average of the corresponding quantities associated with the σ_o measurements used in the 50-km resolution wind cell. The α, β, and γ values (coefficients of residual variance) associated with $\overline{\sigma}_o$ are defined as

$$\overline{Y} = \frac{1}{M^2} \sum_{i=1}^{M} Y_i \tag{28}$$

where $Y_i = \alpha_i$, β_i, or γ_i. The four preaveraged σ_o measurements and associated parameters were then used to estimate the wind using each of the seven algorithms. This preaveraging process reduces the chance of having negative σ_o data (which cannot be used by the WLSL and LWSS algorithms) as well as reduces the computational load significantly. The simulation results for this case are shown in Table V. Comparing the results shown in Table V and the corresponding results shown in Tables II and III, one can observe that with the preaveraging process,

(R1) the performance of the WLSL algorithm degraded at near swath but improved at mid and far swaths;

(R2) the performances of the ML and AWLS algorithms degraded at near swath but remained unchanged at mid and far swaths;

(R3) the performance of the LS algorithm remained unchanged;

(R4) the performances of the WLS, L1 norm and LWSS algorithms improved.

The reason for (R4) may be explained as follows: the computed weights (δ_i) (see Section III) of the residuals (e_i) for the WLS, L1, and LWSS algorithms were more accurate estimates of the variances of the residuals using the preaveraged σ_o measurements. The LS algorithm does not need to compute any weights, so it is insensitive (R3) to the preaveraging process. The degradation of the ML and AWLS algorithms (R2) is due to a lack of knowledge about the probability density function of the preaveraged σ_o measurements. For the WLSL algorithm, the effects of the preaveraging process are not clear. Since the performance of the ML and AWSL algorithms (ranked first and second in Table IV) degraded and the performance of the WLS, L1, and LWSS algorithms improved, the relative performances of all algorithms are even more uniform when preaveraged data is used. The L1 norm algorithm performed best rather than the ML algorithm when preaveraged data is used. Finally, from Tables II, III, and V, in comparing the ML algorithm with no preaveraging

TABLE IV
RANKS FOR EACH ALGORITHM

	Fixed wind speeds and random directions		Random wind speeds and random directions	
ALG.	25 KM	50 KM	25 KM	50 KM
WLSL	3	3	3	3
ML	2	1	3	1
LS	5	5	4	4
WLS	5	5	4	4
AWLS	4	2	2	2
L1	1	4	1	4
LWSS	4	4	4	4

TABLE V
PERFORMANCE RESULTS (m/s) BY PRREAVERAGING THE DATA OBTAINED FROM EACH ANTENNA BEAM

ALG.	50 KM					
	NEAR	MID	FAR	NEAR	MID	FAR
	wind speed 3 m/s			wind speed 25 m/s		
WLSL	0.90	0.76	1.30	4.40	3.54	4.29
ML	0.95	0.68	1.09	4.41	3.55	4.14
LS	1.05	0.67	1.10	4.66	4.09	4.81
WLS	0.95	0.68	1.10	4.51	3.69	4.35
AWLS	0.98	0.68	1.10	4.46	3.56	4.17
L1	0.82	0.55	0.88	4.24	3.21	3.76
LWSS	0.94	0.79	1.42	4.44	3.55	4.27
	wind speed 8 m/s			random wind speed		
WLSL	1.69	0.88	0.97	1.83	1.12	1.32
ML	1.71	0.88	0.98	1.84	1.11	1.22
LS	1.95	1.08	1.21	2.05	1.34	1.52
WLS	1.76	0.91	1.01	1.90	1.14	1.27
AWLS	1.75	0.88	0.98	1.88	1.12	1.23
L1	1.60	0.81	0.89	1.75	0.99	1.11
LWSS	1.72	0.88	0.97	1.85	1.12	1.35

(ranked best) with the L1 norm algorithm with preaveraging (ranked best), one can see that the ML algorithm is better at the near swath location, and worse at the mid and far swath locations.

We have repeated the above simulations using the geophysical model function reported by Wentz *et al.* [3]. Similar conclusions were obtained.

V. DISCUSSION AND CONCLUSIONS

In this paper, we have presented a comparative study of seven wind estimation algorithms using simulated scatterometer σ_o measurements. We have presented the rationale for the weights used in each algorithm. The performance of each algorithm was based on the rms wind vector error. From the simulation results, although the ML algorithm is ranked the best for 50-km wind vector cell resolution (with 16-σ_o measurements) and the L1 norm algorithm is ranked the best for 25-km resolution (with 4-σ_o measurements), performances of all algorithms are quite comparable.

We have also presented results when the σ_o measurements within a 50-km wind cell obtained from each antenna beam were preaveraged and then used to estimate the wind. The results showed that performances of all algorithms were closer to each other. The L1 norm algorithm performance ranks best, rather than the ML algorithm. We feel that these conclusions will not differ significantly if a different preaveraging process is used.

The simulation results presented are based on the current projected NSCAT instrument performance. After the instrument fabrication is completed, its performance may be different from the present estimated performance. For instance, the transmit path loss and the noise figure of the receiver may improve (i.e., smaller), the antenna gain pattern may vary, etc.. The coefficients β and γ in the noise variance will be different for different SNR's. We have performed another set of simulations for the case in which the system SNR was arbitrarily changed by +2 db and another case by −2 db. The same conclusions were drawn regarding the relative performance of the algorithms. Based on these results, preaveraging the data and then estimating the wind using the L1 algorithm is potentially a good approach for NSCAT data processing from both the computational and performance points of view.

We note that the WLSL and LWSS algorithms have the limitation of using only positive data. Although they have such a limitation, their performances are not significantly worse than any other algorithms except for the low wind speed case (corresponding to low SNR—which leads to more negative measurements). Due to the existence of the closed form solutions for wind speed, they are computationally faster than the other algorithms. The solutions associated with these two algorithms are candidates for initializing the other nonlinear wind estimation algorithms if there is a strong constraint on computational load. However, for low SNR cases, they may not be adequate to generate good initial solutions. One can check the quality of the initial guesses by computing the second derivative (Hessian) of the chosen objective function for the solutions associated with these two algorithms. If the second derivative is less than zero, it implies that the initial solution is not in the vicinity of the local minimum of the chosen objective function. In this case, other initial solutions must be obtained; for instance, a binary search over the maximum wind speed range that can be determined from the σ_o measurements with the upwind and down directions. Therefore, we envision the following two-stage wind estimation method. It retrieves the wind first by use of a computationally fast wind estimation algorithm such as the WLSL algorithm. If the estimated wind speed is more than a threshold (e.g., 6 m/s) the accuracy of the estimated wind may be deemed to be sufficient and further refinement using a nonlinear wind estimation algorithm is not required. Otherwise, this estimated wind is used as the initial condition for the nonlinear wind estimation algorithm to improve the wind estimation. From both the computation and wind estimation accuracy points of view this method is useful.

Research on the geophysical model function is proceeding. In the future the commonly accepted model function may not allow any closed form solution. The computational load will then be about the same for any wind estimation algorithm. However, preaveraging of the data is still a good approach.

The seven algorithms studied here obviously do not include all possible wind estimation algorithms. They are just the more popular ones in the estimation field. However, we do believe that they form a representative set of wind estimation algorithms.

REFERENCES

[1] W. L. Jones, L. C. Schroeder, D. H. Boggs, E. M. Bracalente, R. A. Brown, G. J. Dome, W. J. Pierson, and F. J. Wentz, "The SEASAT-A satellite scatterometer: The geophysical evaluation of remote sensed wind vectors over the ocean," *J. Geophys. Res.*, vol. 87, no. C5, pp. 3297–3317, Apr. 1982.

[2] L. C. Schroeder, D. H. Boggs, G. J. Dome, I. M. Halbertsam, W. L. Jones, W. J. Pierson, and F. J. Wentz, "The relationship between wind vector and normalized radar cross section used to derive

SEASAT-A satellite scatterometer winds," *J. Geophys. Res.*, vol. 87, no. C5, pp. 3318–3336, 1982.

[3] F. J. Wentz, S. Peterherych, and L. A. Thomas, "A model function for ocean radar cross sections at 14.6 GHz," *J. Geophys. Res.*, vol. 89, no. C3, pp. 3689–3740, 1984.

[4] F. K. Li, P. Callahan, D. Lame, and C. Winn, "NASA scatterometer on NROSS-A system for global observations of ocean winds," in *Proc. IGARSS* (Strasbourg, France), Aug. 1984.

[5] C-Y. Chi, D. G. Long, and F. K. Li, "Radar backscatter measurement accuracies using digital doppler processors in spaceborne scatterometers," *IEEE Trans. Geosci. Remote Sensing*, vol. GE-24, no. 3, pp. 426–437, May 1986.

[6] C-Y. Chi, R. Aroian, and F. K. Li, "Simulation studies for the NASA scatterometer on NROSS," presented at IGARSS, Zurich, Switzerland, Sept. 1986.

[7] J. M. Mendel, *Discrete Techniques of Parameter Estimation.* New York: Marcel Dekker, 1973.

[8] W. J. Pierson, "A Monte Carlo comparison of the recovery of winds near upwind and downwind from the SASS-I model function by means of the sum of squares algorithm and a maximum-likelihood estimators," NASA Contractor Rep. 3839, Oct. 1984.

[9] H. W. Sorenson, *Parameter Estimation.* New York: Marcel Dekker, 1980.

[10] H. L. Taylor, S. Banks, and J. McCoy, "Deconvolution with the L1 norm," *Geophysics*, vol. 44, pp. 39–53, 1979.

[11] D. M. Marquardt, "An algorithm for least-square estimation of nonlinear parameters," *J. Soc. Indust. Appl. Math*, vol. 11, pp. 431–441, 1963.

[12] C-Y. Chi, J. M. Mendel, and D. Hampson, "A computationally fast approach to maximum-likelihood deconvolution," *Geophysics*, vol. 49, no. 5, pp. 550–565, May 1984.

*

Chong-Yung Chi (S'83–M'83) was born in Taiwan, Republic of China, on August 7, 1952. He received the B.S. degree from the Tatung Institute of Technology, Taipei, Taiwan, in 1975, the M.S. degree from the National Taiwan University, Taipei, Taiwan, in 1977, and the Ph.D. degree from the University of Southern California, Los Angeles, CA in 1983, all in electrical engineering.

In September 1979 he was appointed a Teaching/Research Assistant, and later became a Research Assistant in the Department of Electrical Engineering Systems at the University of Southern California. Since July 1983 he has been with the Jet Propulsion Laboratory, Pasadena, CA. Currently, he is engaged in the studies of spaceborne radar scatterometer systems, SAR processing systems, and deconvolution of radar altimeter signals. His research interests include digital signal processing, image processing, deconvolution, adaptive filtering, system identification, and estimation theory.

*

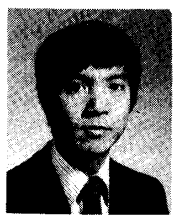

Fuk K. Li was born in Hong Kong in 1953. He received the B.Sc. and Ph.D. degrees in physics from the Massachusetts Institute of Technology, Cambridge, in 1975 and 1979, respectively.

He joined the Jet Propulsion Laboratory, California Institute of Technology, in 1979 and has been involved in various radar remote-sensing activities. He has developed a digital SAR processor/simulator, investigated the tradeoffs of various SAR image quality parameters, and developed several techniques for SAR Doppler parameter estimations. Since 1983, he has also been involved in the design and research studies of airborne and spaceborne scatterometers for remote sensing of ocean winds. He is at present the supervisor of the Radar System Science and Engineering Group. His group activities include: system design and engineering support for the NASA scatterometer, an airborne scatterometer and a rain mapping radar, system design for future spaceborne radars such as a Titan mapping radar, imaging altimeter, advanced scatterometer, etc., and electromagnetic scattering studies, especially those related to multipolarization SAR's.